J. Opt. B: Quantum Semiclass. Opt. **2** (2000) 393–398. Printed in the UK PII: S1464-4266(00)09622-1

Pattern formation and competition in a nonlinear ring cavity

S L Lachinova and W Lu

Department of Physics, Heriot-Watt University, Edinburgh, EH14 4AS, UK

E-mail: PHYSL.phy.hw@phyfsa.phy.hw.ac.uk

Received 17 November 1999, in final form 24 February 2000

Abstract. Spontaneous pattern formation and competition in a nonlinear ring cavity are studied. Complex patterns arising from static and Hopf bifurcations and Hopf–static interactions have been numerically observed and analysed. Among them are flower-like patterns, alternating rolls and oscillating hexagonal structures.

Keywords: Pattern formation, optical instabilities, spatiotemporal dynamics, delay

1. Introduction

Spontaneous pattern formation in nonlinear systems far from equilibrium is currently a topic of considerable interest in many branches of physics [1]. In general, there are two types of bifurcations, Turing (static) and Hopf, which give rise to spontaneous static and dynamical patterns from a homogeneous state respectively. In many nonlinear systems, the two bifurcations can exist and, depending on the control parameters of the systems, one may dominate the other [2–4]. In both situations, simple periodic patterns, such as travelling wave and hexagons, can develop into complex spatial structures on variation of the parameters, due to the presence of the increasing number of active modes [4–10]. On the other hand, in certain parameter domains, the threshold for the two bifurcations may be comparable and, as a result, modes from static and Hopf domains can be active simultaneously. The interaction and competition between static and Hopf instabilities lead to new types of pattern forming phenomena. There are many recent studies of these phenomena in nonlinear systems of a different nature [3, 4, 8, 9]. In optical studies, a typical example is winking hexagons in a single-feedback-mirror configuration [9] due to the resonant interaction between two hexagonal triads of the spatial modes. As a rule, for pattern selections, these modes must satisfy the spatiotemporal phase matching conditions.

In this paper, we study pattern formation and competition in a nonlinear ring cavity. Both static and Hopf instabilities are found to exist in this system and the latter dominates the former on increasing the delay time of the cavity loop. We show a variety of pattern formations in both static and Hopf domains, including flower-like patterns, due to the interaction of modes with different spatial wavelengths, and an alternating roll arising from competition between rolls of the same wavelength but with different orientations. When both static and Hopf modes are active and compete, we observe oscillating hexagonal structures.

2. Mathematical model

The scheme of the passive nonlinear system is shown in figure 1. The ring cavity that is formed by four mirrors is driven by a plane wave. Our mathematical model takes into account a Kerr-type local nonlinear interaction between a light wave and the thin medium with instantaneous response. The transverse interactions arise from the diffusion of the nonlinear slice and diffraction of the light in the resonator. We note that, different from the single pass two-dimensional feedback setting based on a LCLV device [10, 11], the feedback loop in this system is a multi-pass type, which gives rise to richer dynamical features compared with the former configuration. The phase modulation $u(\boldsymbol{r}, t)$ of the propagating light wave in the nonlinear slice is described by the following partial differential equation:

$$\tau_0 \frac{\partial u(\boldsymbol{r}, t)}{\partial t} + u(\boldsymbol{r}, t) = D\nabla_\perp^2 u(\boldsymbol{r}, t) + K|A(\boldsymbol{r}, z = 0, t)|^2 \tag{1}$$

where $\boldsymbol{r} = (x, y)$ is the radius vector in the transverse plane, t is the time coordinate and τ_0 is the characteristic relaxation time of the nonlinearity. D is the diffusion coefficient related to the diffusion length of the nonlinear medium, $\nabla_\perp^2$ the transverse Laplacian and K is the feedback coupling coefficient. $A(\boldsymbol{r}, z = 0, t)$ is the complex amplitude of the intracavity field just before the nonlinear medium.

The field after the nonlinear layer experiences a free-space diffractive propagation in the cavity. This process is described by an ordinary free-propagation equation in the paraxial approximation

$$-2\mathrm{i}k_0 \frac{\partial A(\boldsymbol{r}, z', t')}{\partial z'} = \nabla_\perp^2 A(\boldsymbol{r}, z', t') \tag{2}$$

and two boundary relations of the fields:

$$\begin{aligned} A(\boldsymbol{r}, z' = l, t') &= A(\boldsymbol{r}, z' = 0, t') \exp[\mathrm{i}u(\boldsymbol{r}, t')] \\ A(\boldsymbol{r}, z' = 0, t') &= \sqrt{1 - R} A_{\mathrm{in}}(\boldsymbol{r}) \\ &\quad + R\mathrm{e}^{\mathrm{i}\varphi_0} A(\boldsymbol{r}, z' = L, t') \end{aligned} \tag{3}$$

1464-4266/00/030393+06$30.00

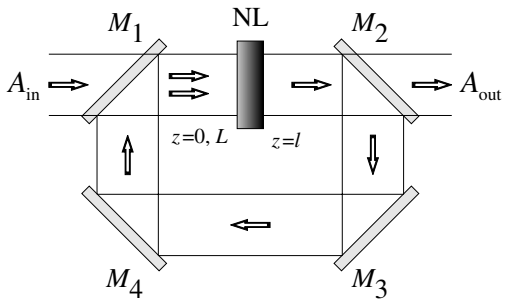

Figure 1. A scheme of the passive nonlinear ring resonator. M_1–M_4 are mirrors with reflectivity coefficients $R_1 = R_2 = R$ and $R_3 = R_4 = 100\%$, NL is the nonlinear medium, L is the resonator length, A_{in} and A_{out} are complex amplitudes of input and output fields, respectively.

where l is the thickness of the nonlinear slice, which is thin and negligible, $k_0 = 2\pi/\lambda$ is the wave number, L is the resonator length and R the reflectivity coefficient of mirrors 1 and 2. φ_0 is a constant phase shift of the light wave in the resonator, τ_R the cavity roundtrip time and $A_{in}(\boldsymbol{r})$ the complex input field amplitude. Note that equations (2) and (3) are written in retarded time variables $\{z' = z, t' = t - z/c\}$ and equation (1) is the same whether the variables are retarded or not, since the thin slice is considered. Combining equations (1)–(3), we obtain the following working equations:

$$\frac{\partial u(\boldsymbol{r},t)}{\partial t} + u(\boldsymbol{r},t) = D\nabla_\perp^2 u(\boldsymbol{r},t) + K|A(\boldsymbol{r},t)|^2 \quad (4)$$

$$A(\boldsymbol{r},t) = \sqrt{1-R}A_{in} + Re^{i\varphi_0}\exp(iL\nabla_\perp^2)\{A(\boldsymbol{r},t-t_R) \times \exp[iu(\boldsymbol{r},t-t_R)]\} \quad (5)$$

where a_0 is the radius of the aperture. We have renormalized these variables $\boldsymbol{r} \equiv \boldsymbol{r}/a_0$, $D \equiv D/a_0^2$, $L \equiv L/2k_0a_0^2$, $t \equiv t'/\tau_0$, $t_R \equiv \tau_R/\tau_0$, $A_{in}(\boldsymbol{r}) \equiv A_{in}$ and $A(\boldsymbol{r}, z' = 0, t') \equiv A(\boldsymbol{r}, t')$.

3. Linear stability analysis

3.1. Steady-state solution

Equations (4) and (5) admit a spatially homogeneous stationary solution. Denoting by u_s and A_s the stationary values of $u(\boldsymbol{r},t)$ and $A(\boldsymbol{r},t)$, respectively, we have

$$u_s = \frac{(1-R)KI_{in}}{1+R^2-2R\cos(u_s+\varphi_0)} \quad (6)$$

where $u_s = K|A_s|^2$ and $I_{in} = |A_{in}|^2$. Equation (6) describes the phenomenon of multistability of the homogeneous stationary state of phase u_s. In the paper, however, we will work in the area of single-valued dependence of u_s with I_{in} for periodical pattern formations.

3.2. Linear stability analysis

For this purpose we perturb the steady-state solution A_s and u_s with $\delta u(\vec{r},t)$ and $\delta A(\vec{r},t)$ and linearize equations (4) and (5) with respect to these perturbations:

$$\frac{\partial}{\partial t}\delta u(\boldsymbol{r},t) + \delta u(\boldsymbol{r},t) = D\nabla_\perp^2\delta u(\boldsymbol{r},t) + K[A_s^*\delta A(\boldsymbol{r},t) + A_s\delta A^*(\boldsymbol{r},t)]$$

$$\delta A(\boldsymbol{r},t) = Re^{i\varphi_0}\exp(iL\nabla_\perp^2)[\delta A(\boldsymbol{r},t-t_R) + iA_s\delta u(\boldsymbol{r},t-t_R)]\exp(iu_s).$$

Expressing the perturbation in a form of spatially modulated wave, $\delta u(\boldsymbol{r},t) = \delta u_0\exp(i\boldsymbol{k}_\perp\boldsymbol{r})e^{\lambda t}$, $\delta A(\boldsymbol{r},t) = \delta A_0\exp(i\boldsymbol{k}_\perp\boldsymbol{r})e^{\lambda t}$, we derive a characteristic equation for determining parameter domains in which spatial pattern formation emerges from a homogeneous state. Here $\boldsymbol{k}_\perp = (k_x, k_y)$ is the transverse wavevector, λ is the perturbation amplification rate. The characteristic equation has the following form:

$$\left(1+\lambda+\frac{D}{L}\theta\right) + \frac{2Ru_s\sin(u_s+\varphi_0-\theta)}{e^{\lambda t_R}+e^{-\lambda t_R}R^2-2R\cos(u_s+\varphi_0-\theta)} = 0 \quad (7)$$

where $\theta = k_\perp^2 L$ is the diffraction parameter.

The boundaries of the instability domains in the plane (θ, u_s) are determined by $\mathrm{Re}\,(\lambda) = 0$ in equation (7). Substituting $\lambda \equiv \lambda + i\omega$ into equation (7) and separating real and imaginary parts of the equation, we obtain for $\lambda = 0$:

$$\begin{cases} \left(1+\dfrac{D}{L}\theta\right)[(1+R^2)\cos(\omega^{th}t_R) \\ \quad -2R\cos(u_s^{th}+\varphi_0-\theta)] \\ \quad -\omega^{th}(1-R^2)\sin(\omega^{th}t_R) + 2Ru_s^{th} \\ \quad \times\sin(u_s^{th}+\varphi_0-\theta) = 0 \\ \omega^{th}[(1+R^2)\cos(\omega^{th}t_R) - 2R\cos(u_s^{th}+\varphi_0-\theta)] \\ \quad +\left(1+\dfrac{D}{L}\theta\right)(1-R^2)\sin(\omega^{th}t_R) = 0. \end{cases} \quad (8)$$

Typical dependences of $u_s^{th}(\theta)$ are periodical with the period equal to 2π. Figures 2(*a*)–(*d*) show the first period in which there are two kinds of instability domains, static (or Turing) and Hopf. In general, the static domains ($\omega = 0$) are independent of the delay time t_R whereas the Hopf domains ($\omega \neq 0$) are absent at $t_R = 0$. Equation (8) has an infinite number of roots for $\omega \neq 0$ and the threshold values u_s^{th} for these roots decrease with the increase of t_R. This can be seen when comparing figure 2(*a*) with figure 2(*c*). The Hopf domains may be separated into odd and even families in terms of their symptomatic frequencies for $t_R \to \infty$: odd for $\omega^{th}t_R \to \pm(2n-1)\pi$ and even for $\omega^{th}t_R \to \pm 2n\pi$, $n = 1, 2, \ldots$. Furthermore, for $t_R \to \infty$, all the instability domains have the same shape. Note that figures 2(*b*) and (*d*) are symmetrical on the horizontal axis. The instability domains can move along the horizontal axis on the variation of the control parameters R and φ_0. Because of this, the relative placement of the Hopf and the static domains can be altered, which gives us a greater possibility of selecting different pattern formations.

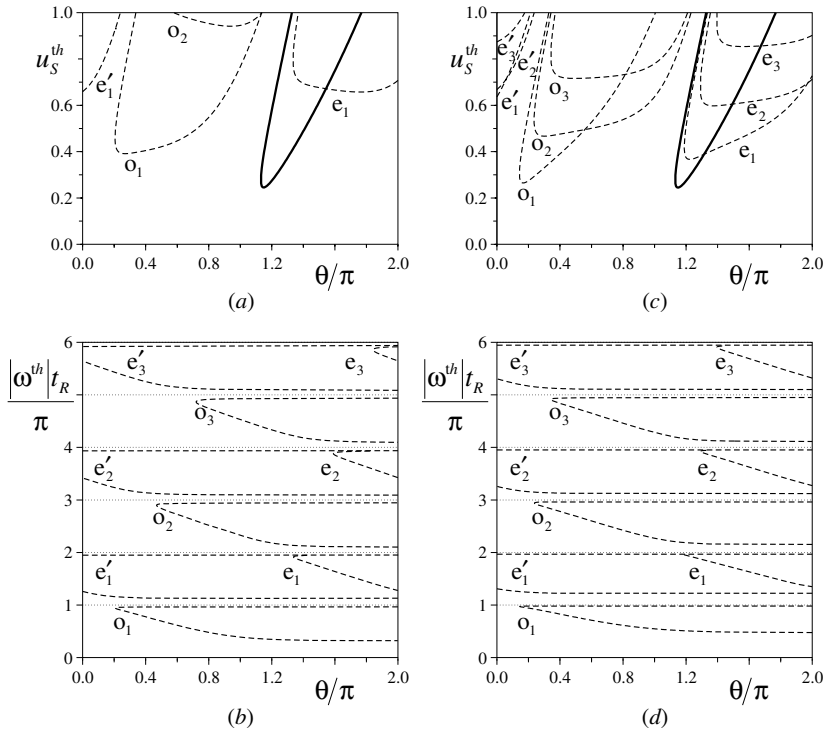

Figure 2. The bifurcation diagrams for $R = 0.8$, $\varphi_0 = \pi$ and $D/L = 0.025$. $t_R = 2$ for traces (*a*) and (*b*) and $t_R = 5$ for traces (*c*) and (*d*). The solid curves in (*a*) and (*c*) mark the static instability domains with $\omega = 0$, whereas the dashed curves give Hopf instability boundaries. Odd families are marked by 'o' and even families are noted by 'e'; their corresponding frequencies are given in trace (*b*) and (*d*).

4. Numerical results and analysis

4.1. Static structures

For relatively short delay, as in figure 2(*a*), the static instabilities dominate. In this case the formation of numerous static patterns takes place beyond the threshold. Formation of the simplest structures, such as the hexagon and the roll, occur due to mode interaction within one instability domain. For this case the number of amplitude equations, which describe the dynamics of these patterns, can be reduced to three for the most unstable static modes. However, on increasing the input intensity or decreasing the value D/L, the number of active modes from other instability domains can join in the pattern forming process, as shown in figure 3(*a*) for five static instability domains, and simple periodic patterns can develop into complex spatial structures. For example, if the excitation condition is fulfilled for two neighbouring static instability domains, spatial patterns, such as an interlaced pattern or a dodecagon, may form in the system [6, 7]. Here the resonant conditions between wavevectors from different domains play an essential role in determining which modes are presented in these patterns. The resulting pattern is a product of competition between basic and complex structures. From an instability point of view, it seems that a further increase in the number of instability domains may lead to the formation of incredibly complicated patterns. However, if the resonant criterion between spatial frequencies from the first and following static instability domains is taken into consideration, the number of possible structures is in fact not so high. This is because the nonlinear system itself will exclude those 'inconvenient' modes from the interaction.

In order to check our theoretical predictions, numerical calculations were performed. To integrate equation (4), we used an alternating direction implicit (ADI) method. The dynamics of the complex amplitude of the intracavity field (equation (5)) were modelled using the generalized Ikeda's map with the fast Fourier transform (FFT) algorithm. The data were stored for a time interval, t_R, to take into account the field delay in the feedback loop. Calculations were performed with small-noise initial conditions and on a transverse square space with grid points $N = 256$. For the case of short delay the obtained results were checked with $N = 512$. The sizes of the transverse domains are adjusted according to different pattern formations for optimal simulation results. All types of structures mentioned above were shown to exist. Figure 3(*b*) shows an example arising from the multi-domain interaction. The corresponding vector diagram, representing a spatial spectrum, is shown in figure 3(*c*). This beautiful pattern formation consists of 'flowers' with six 'petals'. We refer to it as a flower-like pattern though we note that this term was originally introduced for a different type of pattern [12]. For these structures the resonant relations $\boldsymbol{q}^{(1)}+\boldsymbol{q}^{(3)}+\boldsymbol{q}^{(4)} = 0$ and $\boldsymbol{q}^{(1)} + \boldsymbol{q}^{(4)} + \boldsymbol{q}^{(5)} = 0$ are fulfilled; at the same time there is no resonant condition for $\boldsymbol{q}^{(2)}$ and as a result the second domain does not contribute to the pattern formation.

4.2. Hopf structures

By increasing the delay time, for example $t_R > 5$ for $R = 0.8$, $\varphi_0 = \pi$ and $D/L = 0.025$, as in figure 2, the odd Hopf domain, o_1, has the lowest threshold and patterns resulting from the interaction of Hopf modes within this domain emerge. In this case we shall only analyse the Hopf

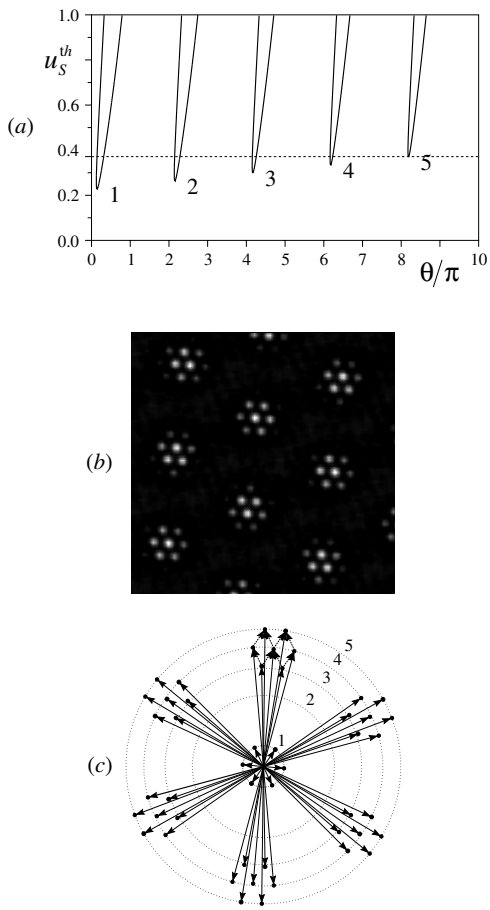

Figure 3. (*a*) The bifurcation diagram for $R = 0.8$, $\varphi_0 = 0$, $D/L = 0.025$ and $t_R = 0$, showing five static instability domains. (*b*) A snapshot of a flower-like pattern in the transverse plane for $I_0 = 0.3$, $K = 1$ ($u_s \cong 0.39$): only one-ninth of the domain simulated is shown. (*c*) The corresponding wavevector diagram.

instabilities. We note that the resonance conditions cannot be fulfilled for the modes within the domain o_1 and hence the basic patterns are travelling or standing waves. If we denote amplitudes of the Hopf modes as $H_n^{\pm}\exp[\mathrm{i}(\boldsymbol{k}_n r \pm \omega t)]$, where $|\boldsymbol{k}_n| = k_H \forall n$, the amplitude equations for them can be written in the following form:

$$\begin{aligned}
&\frac{\mathrm{d}H_n^+}{\mathrm{d}t} + \left(1 + \frac{D}{L}\theta_H\right) H_n^+ = (\mu - \mathrm{i}\omega) H_n^+ \\
&\quad -[\zeta^{(1)}|H_n^+|^2 + 2\zeta^{(1)}|H_n^-|^2 + 2\zeta_{nm}^{(2)}(|H_m^+|^2 \\
&\quad +|H_m^-|^2)]H_n^+ + 2\zeta_{nm}^{(2)} H_m^+ (H_m^-)^* H_n^- \\
&\frac{\mathrm{d}H_n^-}{\mathrm{d}t} + \left(1 + \frac{D}{L}\theta_H\right) H_n^- = (\mu^* + \mathrm{i}\omega) H_n^- \qquad (9) \\
&\quad -[(\zeta^{(1)})^*|H_n^-|^2 + 2(\zeta^{(1)})^*|H_n^+|^2 \\
&\quad +2(\zeta_{nm}^{(2)})^*(|H_m^-|^2 + |H_m^+|^2)]H_n^- + 2(\zeta_{nm}^{(2)})^* H_m^- (H_m^+)^* H_n^+
\end{aligned}$$

where $n = 1, \ldots, M$, $M \leqslant 2$ and $\theta_H = k_H^2 L$. The complex coefficient, $\zeta_{nm}^{(2)}$, depends on the angle between $\boldsymbol{k}_n$ and $\boldsymbol{k}_m$. The number of interacting modes M may vary. If $M = 1$, equations (9) describe the formation of basic Hopf structures such as the travelling wave and the standing wave. More complicated Hopf structures emerge for $M = 2$ due to a combination of travelling waves. One example of interesting dynamical patterns is alternating rolls, snapshots

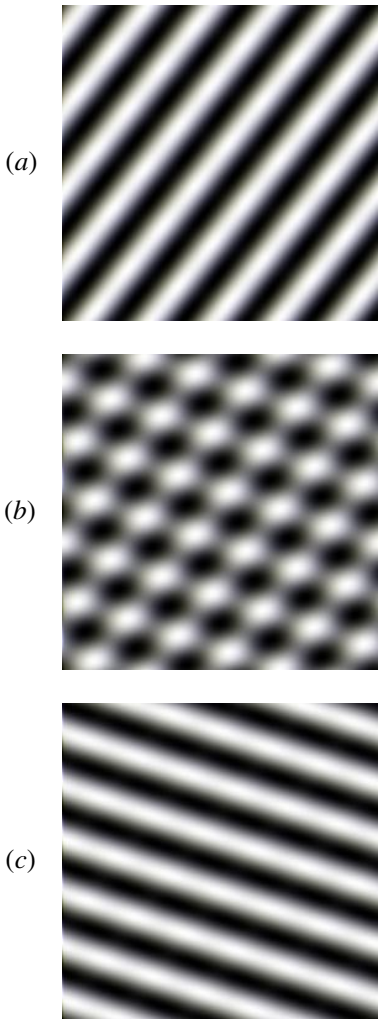

Figure 4. Alternating rolls for three different times (*a*)–(*c*). Parameters are $R = 0.4$, $\varphi_0 = 0.4\pi$, $D/L = 0.1$, $t_R = 5$, $I_0 = 3.7$, $K = 1$.

of which are shown in figure 4. Alternating rolls arise due to nonlinear interaction of two standing waves with different plane orientation and a phase shift of π.

4.3. Hopf–static structures

The resonant conditions for frequencies of interacting modes can further be fulfilled for modes that belong to different types of instability domains, namely Hopf and static. In this case static and Hopf modes can join together in the pattern forming process. Figure 2(*c*) is an example in which Hopf and static bifurcations have comparable threshold values. The simplest structure for this case is the triadic Hopf–static (THS) pattern [3] as shown in figure 5(*a*), with the corresponding vector diagram in 5(*b*). The wavevectors $\boldsymbol{k}_1$ and $\boldsymbol{k}_2$, $|\boldsymbol{k}_1| = |\boldsymbol{k}_2| = k_H$, belong to the Hopf instability domain, whereas the wavevector $\boldsymbol{q}$, $|\boldsymbol{q}| = q_s$, corresponds to the static mode. The resulting pattern drifts in the direction perpendicular to $\boldsymbol{q}$. A more complicated Hopf–static structure is winking hexagons, which consist of two hexagonal triads from Hopf and static domains. In this pattern formation the brightness of the individual components

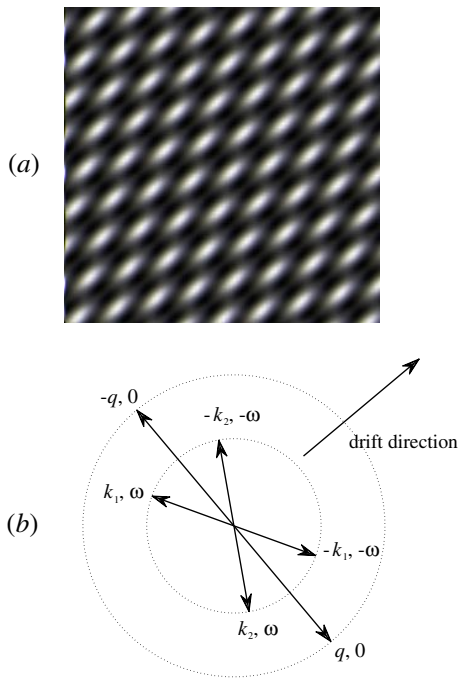

Figure 5. (*a*) A snapshot of the triadic Hopf–static pattern. (*b*) The corresponding wavevector diagram for $R = 0.2$, $\varphi_0 = 0.13\pi$, $D/L = 0.025$, $t_R = 10$, $I_0 = 4.8$, $K = 1$.

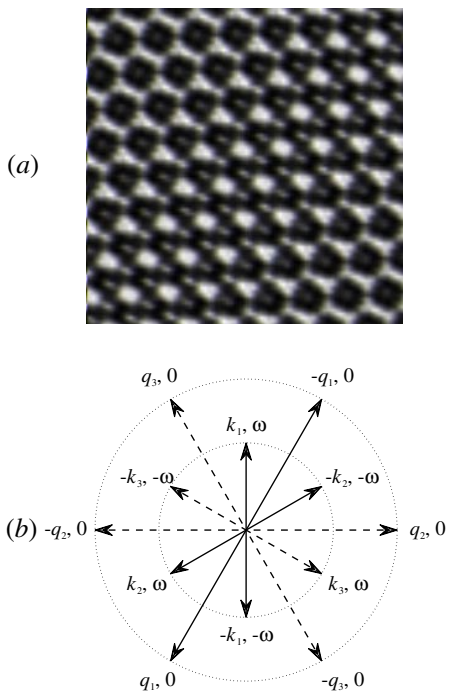

Figure 6. (*a*) A snapshot of the oscillating hexagonal structures. (*b*) The corresponding wavevector diagram for $R = 0.2$, $\varphi_0 = 0.15\pi$, $D/L = 0.025$, $t_R = 10$, $I_0 = 4.8$, $K = 1$.

oscillates in time [9]. For winking hexagons the relation $q_s^2 = 3k_H^2$ is required. However, a small deviation from this relation can lead to the interruption of symmetry and, as a result, the amplitude of one triad is slightly stronger than that of the other. The resulting pattern (figure 6) shows the evolutionary feature of winking hexagons in different local regions of the transverse plane and it drifts in the direction perpendicular to the strongest static wavevector $\boldsymbol{q}$. We note that such structures are observed only in a very narrow area of the control parameters R and φ_0 because the above relation is fulfilled in the vicinity of the spatial-homogeneous phase multistability region in which the system often leads to a spontaneous jump to localized states [14] or chaotic structures when the amplitude of the pattern is large. To avoid this jump, calculations were performed very close to the threshold and with a small value of diffusion coefficient, since the increase of diffusion coefficient leads to the decrease of distance between the threshold value and the second bistability branch.

In summary, we have observed complex spatial structures of the optical field, such as flower-like patterns, alternating rolls and oscillating hexagonal structures, which arise from static and Hopf bifurcations, and Hopf–static interactions in a nonlinear ring cavity. Here the mechanism responsible for periodic and quasiperiodic pattern formation is in principle the same as many other nonlinear diffractive systems [3–6, 8, 9], namely resonant interactions for active modes. The delay feedback often leads to the appearance of dynamical resonance interactions that satisfy the matching of temporal frequencies of the interactive modes. In this case, similar dynamical structures can also be observed in different nonlinear systems. However, in many of these systems, for example a single-feedback-mirror device with counter-propagating waves [3] or a ring cavity with a dispersive quasi-Kerr medium [15], the relations between spatial critical wavelengths from different instability domains are fixed and not dependent on the control parameters of the system. Our model, however, is flexible in these relations with the choice of control parameters R and φ_0. As a result, types of quasiperiodic pattern may vary with R and φ_0; an example being the transition from dodecagon to flower-like patterns on the variation of φ_0. Moreover, with the increase of delay time, more Hopf modes in our system with higher frequencies will participate in the pattern formation process. Consequently the complexity of the spatio-temporal structures can only be limited by imagination and computation/resolution. The possibility of new pattern formations such as a 'winking dodecagon' type of pattern is currently under investigation.

Acknowledgment

This work is supported by EPSRC (UK) Grant No GR/M32573.

References

[1] Lugiato L A, Brambilla M and Gatti A 1998 *Optical Pattern Formation (Advances in Atomic, Molecular and Optical Physics)* ed B Bederson and H Walther (London: Academic)
Arecchi F T, Boccaletti S and Ramazza P L 1999 *Phys. Rep.* **318** 1–83
[2] Patrascu A S, Nath C, Le Berre M, Ressayre E and Tallet A 1992 *Opt. Commun.* **91** 433–43
[3] Logvin Yu A, Samson B A, Afanas'ev A A, Samson A M and Loiko N A 1996 *Phys. Rev.* E **54** R4548–51
[4] Logvin Yu A and Ackemann T 1998 *Phys. Rev.* E **58** 1654–61
[5] Degtiarev E V and Vorontsov M A 1996 *J. Mod. Opt.* **43** 93–8

[6] Vorontsov M A and Karpov A Y 1997 *J. Opt. Soc. Am.* B **14** 34–50
[7] Ivanov V Yu, Lachinova S L and Iroshnikov N G 1999 *Proc. SPIE* **3733** 204–10
[8] Le Berre M, Leduc D, Patrascu S, Ressayre E and Tallet A 1999 *Chaos Solitons Fractals* **10** 627–49
[9] Logvin Yu A, Ackemann T and Lange W 1997 *Europhys. Lett.* **38** 583–8
[10] Vorontsov M A, Dumarevsky Yu D, Pruidze D V and Shmalhauzen V I 1988 *Izv. Akad. Nauk USSR Fiz.* **52** 374–6
[11] Akhmanov S A, Vorontsov M A and Ivanov V Yu 1988 *JETP Lett.* **47** 611–14
[12] Grynberg G, Maitre A and Petrossian A 1994 *Phys. Rev. Lett.* **72** 2379–82
[13] Silber M, Riecke H and Kramer L 1992 *Physica* D **61** 260–78
Silber M and Knobloch E 1991 *Nonlinearity* **4** 1063–106
[14] Le Berre M, Patrascu A S, Ressayre E and Tallet A 1997 *Phys. Rev.* A **56** 3150–60
[15] Le Berre M, Leduc D, Ressayre E and Tallet A 1996 *Phys. Rev.* A **54** 3428–46